Available online at www.sciencedirect.com
ScienceDirect
International Journal of Thermal Sciences 46 (2007) 491–500
International Journal of Thermal Sciences
www.elsevier.com/locate/ijts

An experimental investigation of the heat transfer in a ribbed triangular cooling channel

M. Amro [a], B. Weigand [a,*], R. Poser [a], M. Schnieder [b]

[a] *Institute of Aerospace Thermodynamics (ITLR), Universität Stuttgart, Pfaffenwaldring 31, D-70569 Stuttgart, Germany*
[b] *Turbine, Cooling and Heat Transfer Alstom (Schweiz) AG, Brown Boveri Strasse 7, CH-5401 Baden, Switzerland*

Received 3 March 2006; received in revised form 16 May 2006; accepted 10 July 2006

Available online 10 August 2006

Abstract

One of the most challenging aspects of gas turbine cooling is the cooling of the first stages of turbine blades. Here the highest external heat load is seen at the leading edge of the blade. The present study investigates the internal cooling in a triangular channel with a rounded edge as a model of a leading edge cooling channel for a gas turbine blade. A transient liquid crystal method is used to measure the heat transfer. Experimental results are reported for a number of new 3D rib configurations for Reynolds numbers between 50 000 and 200 000. From the experimental results it has been found that 60 deg. ribs provide in general higher heat transfer enhancements than 45 deg. ribs. However, this results in extremely high friction factors for the 60 deg. ribs. Taking the local and mean distributions of the heat transfer coefficients (as well as the increase in friction factors) into consideration, it was found that the most promising rib arrangement for leading edge cooling is a 3D rib with 45 deg. angle and double-sided fully overlapped ribs in the arc area. These ribs provide uniform heat transfer in the arc area as well as a high level of the heat transfer coefficients in the channel. The resulting friction factors are in an acceptable range for these ribs.

Keywords: Internal flow; Internal heat transfer; Triangular channel; Gas turbine blade cooling; Heat transfer enhancement; Transient liquid crystal method

1. Introduction

Modern gas turbine blades have to be heavily cooled because of the extremely high turbine inlet temperatures. Because the allowable metal temperature is much lower than the outside hot gas temperature, the blade material temperature has to be lowered by using internal cooling channels and external film cooling. Especially the leading edge region of a turbine blade is exposed to a very hot gas stream and high external heat transfer coefficients. In order to increase the internal heat transfer, turbulence promoters are normally used. Here ribs are very common. These ribs are usually placed in a repeated manner to disturb the boundary layer periodically leading to high turbulence levels and good mixing in the coolant core flow. It has been found that the flow achieves a periodic fully developed state after about five ribs. Because of their importance, a large amount of work has been done in the past and is still continuing to understand the effects of different rib turbulators on the pressure drop and on the heat transfer in channels. The main body of work deals with rectangular channels. This work was summarized and reviewed by e.g. Han and Dutta [1], Taslim [2], Ligrani et al. [3] and in a book by Han et al. [4]. Thereby also the influence of rib spacing, rib angle and rib height has been investigated. Angled ribs introduce swirling motion in the flow and therefore increase mixing as well as local heat transfer. The ribs can be continuous or broken or have a V-shaped form (e.g. Han et al. [5], Han and Zhang [6]). With this, the number of vortices introduced in the core flow can be varied. The resulting secondary flow can be adopted using different rib arrangements on e.g. opposite walls of the cooling channel.

Much less work is known for ribbed triangular channels. Metzger et al. [7], Metzger and Vedula [8] and also Zhang et al. [9] investigated the heat transfer enhancement in a ribbed triangular duct. Haasenritter and Weigand [10] numerically predicted the heat transfer enhancement in a ribbed triangular duct by using a k–ε turbulence model. Good agreement was found

* Corresponding author.
E-mail address: bw@itlr.uni-stuttgart.de (B. Weigand).

1290-0729/$ – see front matter
doi:10.1016/j.ijthermalsci.2006.07.004

Nomenclature

A	flow area	m^2	
c_p	specific heat at constant pressure	$J\,kg^{-1}\,K^{-1}$	
D	hydraulic diameter, $=4A/U$	m	
e	rib height	m	
f	friction factor		
h	heat transfer coefficient	$W\,m^{-2}\,K^{-1}$	
H	channel height	m	
k	thermal heat conductivity	$W\,m^{-1}\,K^{-1}$	
n	normal wall coordinate	m	
Nu_D	Nusselt number, $=hD/k$		
Nu_0	reference Nusselt number, Eq. (6), $=hD/k$		
p	pressure	Pa	
P	rib pitch	m	
Pr	Prandtl number, $=\mu c_p/k$		
R	specific gas constant	$J\,kg^{-1}\,K^{-1}$	
Re_D	Reynolds number, $=\bar{u}D\rho/\mu$		
St	Stanton number, $=Nu_D/(Re_D Pr)$		
t	time	s	
T	temperature	K	
$\bar{u}$	mean flow velocity	$m\,s^{-1}$	
U	wetted perimeter	m	
U_r	length of suction plus pressure side (ribbed perimeter)	m	
x	axial coordinate	m	
α	thermal diffusivity, $=k/(\rho c_p)$	$m^2\,s^{-1}$	
γ, γ_1	rib angle	°	
ξ	coordinate from the wall towards the material	m	
μ	dynamic viscosity	$N\,s\,m^{-2}$	
η	heat transfer efficiency		
ρ	density	$kg\,m^{-3}$	

Subscripts

B	bulk condition
0	initial condition, reference values
min	minimum
w	wall

between the experimental data of Metzger et al. [7] and their numerical calculations. Taslim et al. [11] studied coolant channel shapes relevant for the leading edge of an aero-engine blade for Reynolds numbers up to 30 000. They used a triangular ribbed channel with a rounded side and studied also the effect of ribs on the base plate. However, they used only ribs with a constant height.

Compared to the heat transfer requirements for aero-engine blades, the cooling schemes of blades for large industrial gas turbines differ in some aspects (see e.g. Weigand et al. [12]). An important difference is that blades for heavy-duty gas turbines are subjected to much higher Reynolds numbers in the internal cooling passages mainly due to their much larger dimensions. On the other side, the larger size of the internal cooling passages gives much more freedom for designing the shape of cooling and heat transfer enhancement features like ribs inside the blades. Thereby the rib geometries can be adapted to the actual cooling channel form, which is usually not square or rectangular. Typical examples are the cooling channels near the leading and trailing edge of the blade or channels of aerodynamically optimized blades for later stages (Hall et al. [13]). All these internal cooling ducts might be approximated by triangular channels. Within these channels three-dimensional shaped turbulators can be manufactured for industrial gas turbine blades. Therewith the local heat transfer can be influenced drastically. The rib height is gradually decreased with decreasing channel height. Hall et al. [13] used the criteria, that the local height of the rib e divided by the local channel height H is constant. Applying this criterion, the local friction in the channel between the core region and the apex area can be equalized. This promotes the secondary flow to exchange air between the core area and the apex area, leading to higher heat transfer coefficients in the edges where the heat load from the hot gas side is highest. 3D shaped turbulators can also be used for effectively cooling the leading edge of a gas turbine blade. Fig. 1 shows an example for such an application (Beeck et al. [14]) from a patent. The three-dimensional ribs are additionally angled with respect to the main flow direction and can have different overlapping arrangements in the corner area. Further, the rib spacing can vary, to adopt the heat transfer enhancement to the local cooling requirements. With this, local heat transfer distributions can be tailored along the channel circumference to achieve small temperature differences and hence small thermal stresses within the blade. Very little work has been done up to now on the experimental investigation of these new rib types. Amro et al. [15] presented some first results on an experimental and numerical study of the performance of these ribs. Thus, the aim of the present paper is to investigate the local heat transfer enhancement in a leading edge channel of a gas turbine blade by these new 3D ribs. Especially, it is of high interest to explore the possibility to locally influence the heat transfer in the leading edge by changing and optimizing the rib shape. To the best knowledge of the authors of the present paper, such a detailed study on 3D rib performance in a leading edge channel is not yet available in literature.

2. Experimental setup and measurement methods

A sketch of the experimental setup is given in Fig. 2. The working medium is air, which is supplied to the test section through a vacuum pump. The air enters the settling chamber (2) through a filter (1). The settling chamber reduces the unsteadiness and swirl in the flow and has a length of about 12 hydraulic diameters, D. It is equipped with a laminar flow element (3) to measure the flow rate. It follows a heater (4), which is able to heat up the free stream temperature in 20–30 milliseconds to the desired value of 40–60 °C. The heater is similar to the one described in Wang et al. [16]. An outlet section (6) with a length of $20D$ is attached to the main test channel (5) to avoid

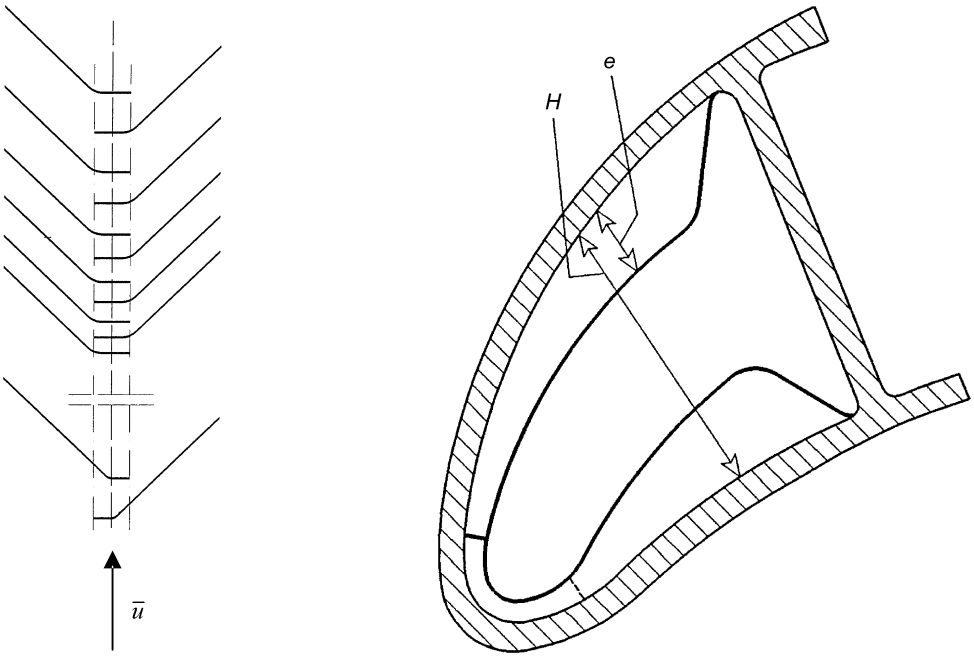

Fig. 1. Three-dimensional turbulators for a leading edge cooling channel of an industrial gas turbine blade (from [14]).

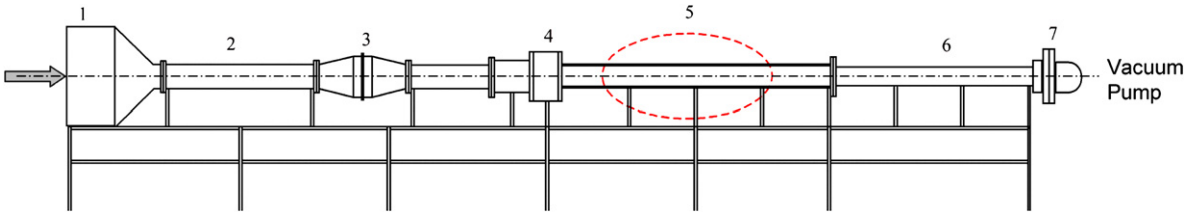

Fig. 2. Sketch of the test facility.

disturbances from the vacuum pump. The test section consists of a $20D$ long triangular duct with a hydraulic diameter D of about 91 mm. It is built of transparent Perspex with a wall thickness of 20 mm. The cross section of the test section is shown in Fig. 3. For the determination of the friction factor and the pressure loss eight pressure taps are placed along the circumference in the inlet section as well as in the outlet section of the duct. Furthermore, there are sixteen pressure taps placed along the base plate of the channel for obtaining the pressure gradient along the test section. The pressure taps were connected by nylon tubes to a Scanivalve DSA 3000 pressure measurement system, which is capable of 128 simultaneous pressure measurements with an accuracy of 0.1% of the measurement range. A multi-channel module records the information of all pressure taps simultaneously. The mass flow has been measured by using a laminar flow element. For the heat transfer measurements a transient liquid crystal technique has been applied. The channel and the fluid have initially room temperature. At $t = 0$ the fluid is exposed to a step change in the free stream temperature by switching the heater on. The surface, where the distribution of the heat transfer coefficient should be measured, is coated with liquid crystals and shows a color change in time. In order to determine the correct driving temperature difference between the wall and the fluid, the centerline temperature in the cross section of the channel is measured at several positions along the

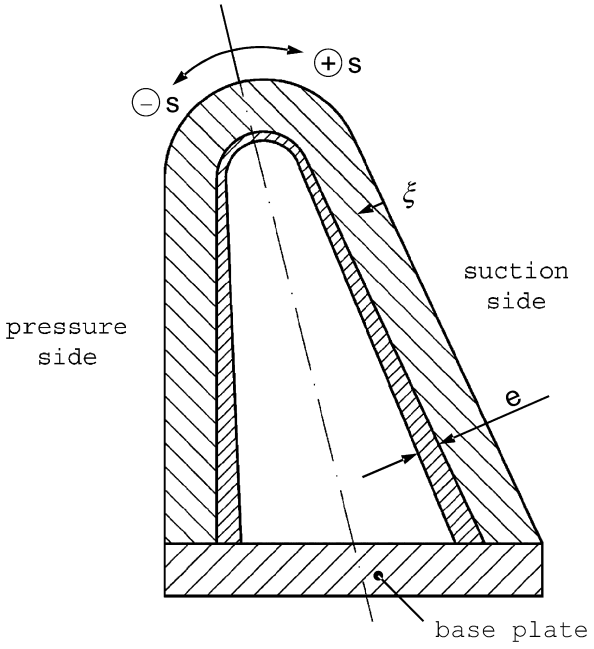

Fig. 3. Cross-section of the duct.

channel. The heat transfer coefficients were measured between two ribs at a distance of 15 to 16 hydraulic diameters from the entrance of the test channel. At this position the flow is assumed

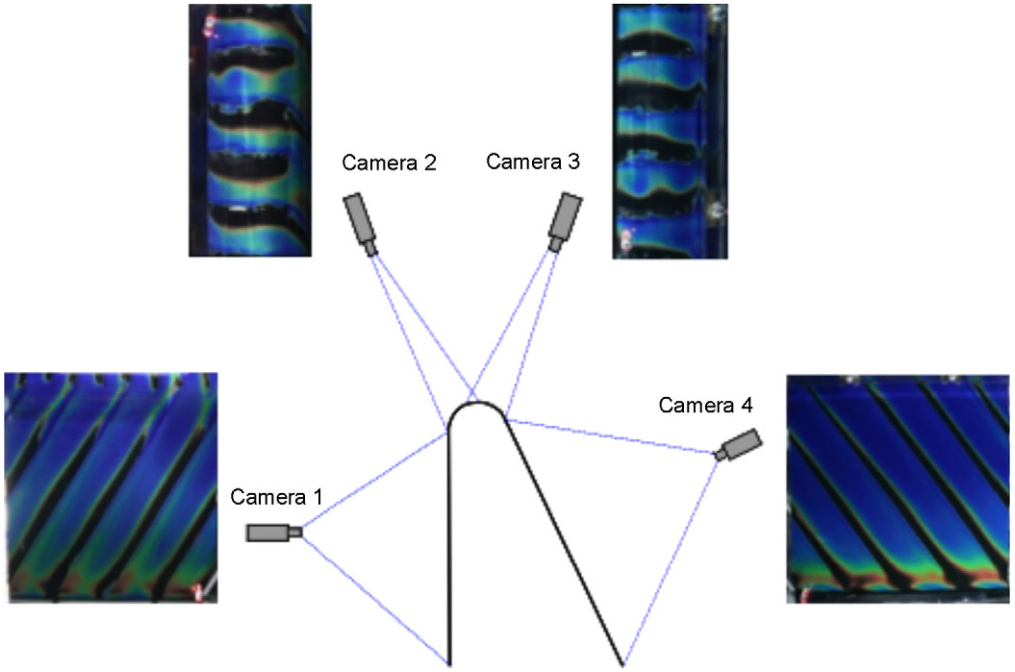

Fig. 4. Camera set up for measuring the wall temperature.

to be fully developed (periodic). The surface temperature evolution is monitored by several CCD cameras. These cameras are fixed around the channel and record the change of color with time. This is shown in Fig. 4. The cameras are able to take 25 pictures per second. For the evaluation of the picture sequence a digital image processing program was used. More information on the image processing program can be found in Vogel [17]. From the measured surface temperature distribution the heat transfer coefficients can be determined. The narrow band liquid crystals used for the tests had a mean indication point at 30 °C and a bandwidth of 1 °C.

2.1. Investigated rib configurations

In order to improve the internal heat transfer, regular rib structures are attached to the inner surface of the duct. They cause a periodic boundary layer separation and re-attachment of the flow, whereas the heat transfer is locally increased. In addition, secondary flow is introduced by the ribs, which causes better mixing. For such rib structures it is well known that the behavior of the flow with respect to the re-attachment areas depends on the ratio between rib pitch P and height e of the ribs. For lower ratios of P/e a closed recirculation area exists between the ribs. If the ratio P/e becomes too large, the boundary layer grows to large values in front of the next rib, which means that further heat transfer enhancement might be inefficient there. That is why in practice often ratios of $7 < P/e < 15$ are preferred [4].

The principal rib geometry has already been shown in Fig. 3. The ribs, which have a locally varying height e in the channel, are placed in a staggered arrangement. Fig. 5 shows the geometrical details of the rib arrangement. The ribs are inclined under an angle γ to the main flow direction. The rib height $e_{\min}$ is reached in the leading edge arc. The angle of the rib in the leading edge arc is given by γ_1. From here, the rib height is linearly increasing towards the base plate (see Fig. 3). The rib shape in the leading edge part of the channel has been varied as well as the rib angle γ. The different variations for the leading edge part of the rib are depicted in Fig. 6. Here basically five cases can be distinguished. Case 1 has no rib in the arc, cases 2 and 3 have a short or a large orthogonal rib in the arc. Case 4 shows a rib, with only one side in the arc, whereas case 5 presents a rib structure with diagonal ribs running around the arc. The rib height in the arc is constant, whereas the rib height e in the channel itself is linearly increasing from $e_{\min}$ to 0.10 or 0.15 H near the base of the channel (see also Figs. 3 and 5). The rib modifications in the arc are important, because high heat transfer coefficients are needed on the inner side of the leading edge. Furthermore, two different dimensionless rib heights $e/H = 0.10$ and 0.15 and two dimensionless pitches $P/e_{\min} = 15$ and 20 have been investigated. Table 1 summarizes all investigated configurations. The different rib configurations have been selected in order to locally improve the heat transfer in the leading edge region. In particular, one aim of the present study was to show the possibility of moving the point of maximum heat transfer coefficient to different positions in the leading edge arc in order to adopt the internal heat transfer coefficients to the external heat load. In addition it was studied, if a rib is needed in the arc area, or if the secondary motion driven by the 3D ribs might be enough to keep high heat transfer coefficients in the arc area by flow impingement.

2.2. Measurement of the pressure loss

The friction factor f for an incompressible flow can be defined by:

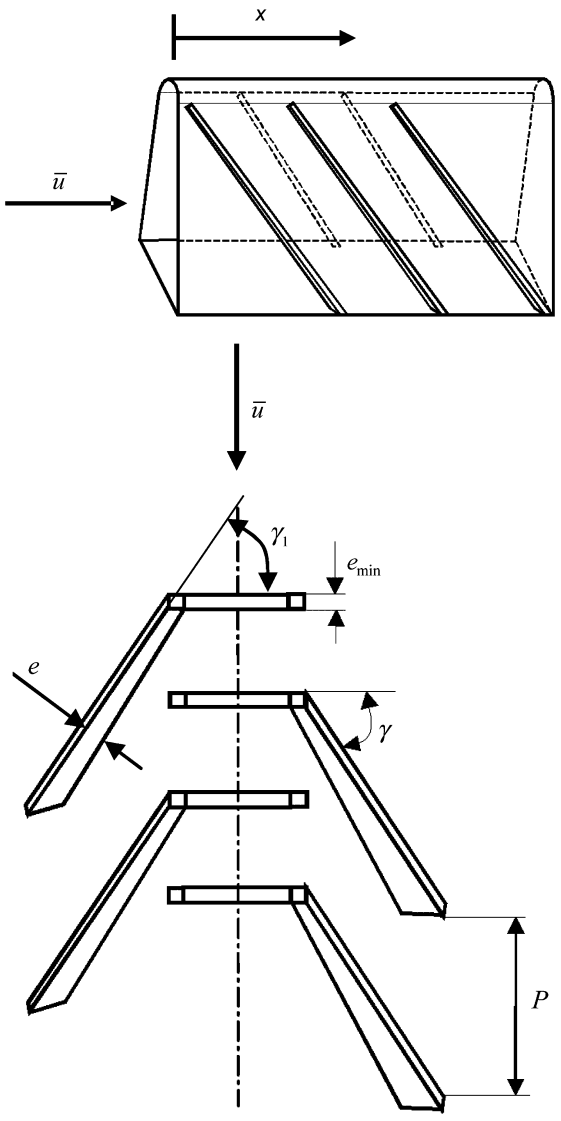

Fig. 5. Rib geometries.

$$f = -\frac{\mathrm{d}p}{\mathrm{d}x}\frac{D}{2\rho\bar{u}^2} \tag{1}$$

The pressure gradient has been determined at sixteen positions along the base plate of the duct. A visual control before evaluating the friction factor f by a linear regression analysis ensured the proper function of every single pressure tap. The obtained friction factor f represents the mean friction in the duct.

2.3. Heat transfer measurements

Heat transfer measurements were performed by using the transient liquid crystal method as described in various previous studies [18,19]. After homogeneous flow and initial temperature conditions were established, a sudden change of the fluid temperature was initiated and the time response of the wall temperature was recorded. The behavior of the wall temperature due to this temperature change can be described for short measurement times by solving the 1D conduction equation for

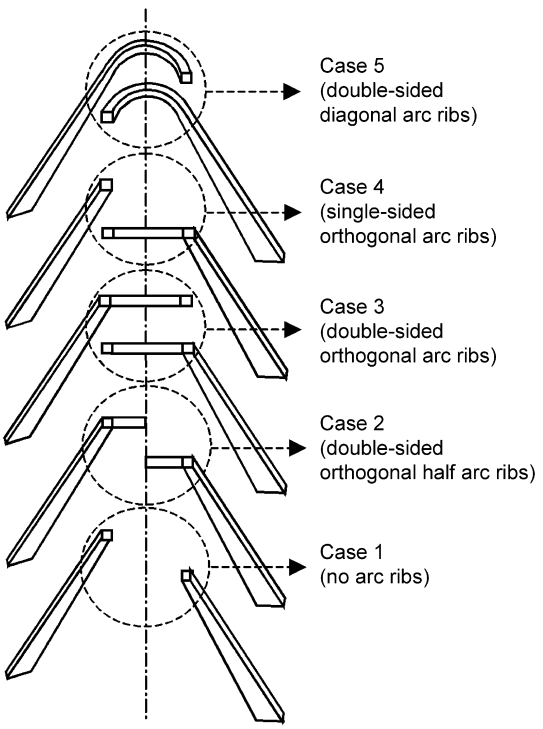

Fig. 6. Detailed rib geometries in the arc area of the leading edge channel.

Table 1
Tested rib geometries

Abbreviation	Rib configuration				
	Ribs			Leading edge arcs	
	γ	P/e_{min}	e/H	γ_1	Comment
Case 1 – 45°	45°	15	0.10	–	without
Case 2 – 45°	45°	15	0.10	90°	double-sided half
Case 5 – 45°	45°	15	0.10	45°	double-sided fully overlapped
Case 3 – 45°	45°	15	0.10	90°	double-sided fully overlapped
Case 4 – 45°	45°	15	0.10	90°	single-sided full
Case 3a – 45°	45°	20	0.10	90°	double-sided fully overlapped
Case 3b – 45°	45°	20	0.15	90°	double-sided fully overlapped
Case 1 – 60°	60°	15	0.10	–	without
Case 5 – 60°	60°	15	0.10	60°	double-sided fully overlapped
Case 3 – 60°	60°	15	0.10	90°	double-sided fully overlapped

an unsteady temperature field with the assumption of a semi-infinite wall.

$$\rho c_p \frac{\partial T}{\partial t} = \frac{\partial}{\partial \xi}\left(k\frac{\partial T}{\partial \xi}\right) \tag{2}$$

with the initial and boundary conditions

$$\begin{aligned} &t = 0: \quad T = T_0 \\ &\xi = 0: \quad -k\frac{\partial T}{\partial \xi} = h(T_W - T_B) \\ &\xi \to \infty: \quad T = T_0 \end{aligned} \tag{3}$$

where T_0 is the initial material temperature, T_B is the bulk temperature in the channel, T_W is the wall temperature, h is the heat transfer coefficient, and α and k are the thermal diffusivity and conductivity of the wall material respectively. The coordinate ξ is measured from the surface towards the material, as indicated

Table 2
Uncertainties in measurement quantities

Quantity	ρ	Re_D	D	t	$T_B - T_0$	$T_W - T_0$
Uncertainty	0.8%	2%	0.8%	1.9%	0.7%	1.8%

in Fig. 3. The solution of Eqs. (2)–(3) results in the following expression for the wall temperature distribution:

$$\frac{T_W - T_0}{T_B - T_0} = 1 - \exp\left(\frac{h^2 \alpha t}{k^2}\right) \operatorname{erfc}\left(\frac{h\sqrt{\alpha t}}{k}\right) \tag{4}$$

This solution is valid only for a step change in fluid temperature. For different changes of the fluid temperature the temperature history may be approximated according to the Duhamel principle [20]. Using the time of the thermal liquid crystal indication and a local time-resolved bulk temperature profile, Eq. (4) may be solved for the heat transfer coefficient.

In deriving Eq. (4), curvature effects of the surface have been ignored. It has proven by the method presented in [21] that these effects are negligible for the present configuration, even in the leading edge part of the channel.

2.4. Measurement uncertainty

Uncertainties related to the pressure and heat transfer measurements were estimated and are shown in Table 2. Uncertainty in the pressure measurements depended strongly on the pressure sensor used and the Reynolds number in the channel. This uncertainty ranged from 0.2% up to 20% for the lowest pressure differences. However, the resulting uncertainty in the slope of the pressure profile along the channel was much lower due to the calculation of the regression of the slope used to determine the pressure loss over the channel. The overall errors in the friction factor were about 4%. Uncertainties in the heat transfer measurements were based on temperature, time, and material property uncertainties. Temperature uncertainties were mainly bias errors as a result of the thermocouple calibration curve used and, thus, were not compounded in the use of a temperature evolution in the evaluation of heat transfer coefficients. Uncertainties in the material properties of the Perspex walls were estimated at 5%, resulting in a total uncertainty in the Nusselt number of about 7%.

3. Results

3.1. Smooth channel

As a reference, the smooth channel has been investigated. Fig. 7 shows the distribution of the local Nusselt number, defined by

$$Nu_D = \frac{-\frac{\partial T}{\partial n}|_W D}{T_W - T_B} = \frac{hD}{k} \tag{5}$$

around the circumference of the channel as a function of the relative position s/U_r. U_r is the length of the wetted perimeter minus the length of the base plate (see Fig. 3), which is the length of the ribbed circumference. In Eq. (5) $(\partial T/\partial n)_W$ denotes the temperature gradient at the wall in normal direction. The point $s/U_r = 0$ of the relative position indicates the zero point of the coordinate system, as shown in Fig. 3. Positive values of the coordinate indicate positions on the suction side, whereas negative values indicate positions on the pressure side. From Fig. 7 it can be seen that the local Nusselt number in the rounded edge of the channel (leading edge) shows a minimum because of the flow restriction in this area. This is clear, because the flow is pushed outwards from the arc area, which is a typical behavior for the flow in triangular ducts (see e.g. Nikuradse [22]). The mean value of the Nusselt number for the smooth channel can be predicted with good accuracy by the Dittus–Boelter correlation [23], given by

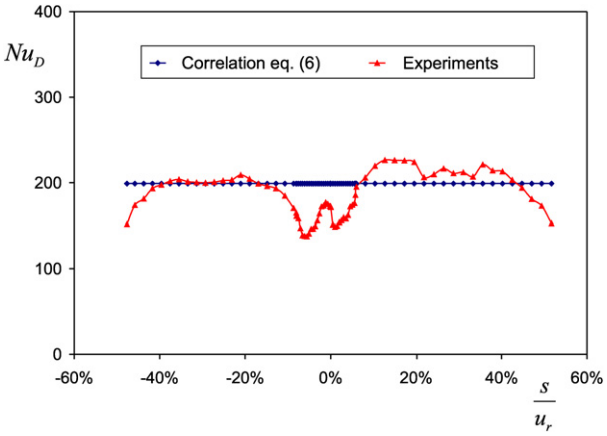

Fig. 7. Local Nusselt number distribution for the smooth channel.

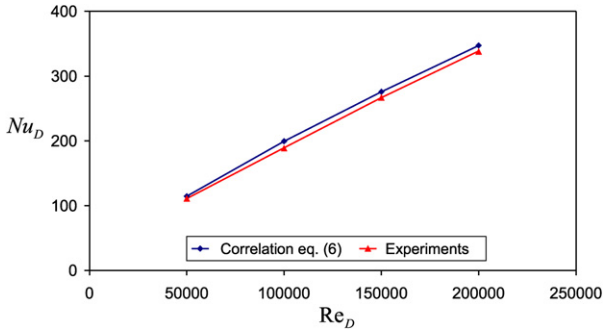

Fig. 8. Averaged Nusselt number for the smooth channel as a function of the Reynolds number.

$$Nu_0 = 0.023 Re_D^{0.8} Pr^{0.4} \tag{6}$$

This is shown in Fig. 8 for a range of Reynolds numbers from 50 000 to 200 000. For obtaining the Nusselt number, the evaluation method of von Wolfersdorf et al. [24] has been used to obtain the correct driving temperature difference $(T_W - T_B)$ from the measured wall temperatures and centerline temperatures.

The friction factor in the smooth channel coincides by about 5% with the Blasius friction factor

$$f_0 = 0.046 Re_D^{-0.2} \tag{7}$$

Therefore, the following results for the ribbed channel will be based on Eqs. (6)–(7) for the friction factor and for the Nusselt

number. This has the advantage that the overall heat transfer enhancement compared to a smooth channel can be visualized. Furthermore it has to be mentioned that special focus was given to the possibility to enhance the low heat transfer coefficients in the leading edge part of the channel. Here different possibilities will be explained afterwards.

3.2. Ribbed channel with different rib geometries

First of all individual rib characteristics regarding friction loss and heat transfer will be discussed. Here a lot of different geometric configurations are tested. The geometries are given in Table 1 and are shown in Fig. 6. The basic configurations (cases 1–5) have different rib configurations in the arc area of the leading edge. Tests have been done for rib angles of 45° and 60°. In order to investigate later the rib performance, the pressure loss and the heat transfer need to be discussed first.

3.2.1. Pressure drop

Each rib structure, which is inserted into a duct, results in an obstruction of the flow. In this case all investigated rib structures cause a regular boundary layer separation and re-attachment. This is reflected in an increased pressure drop and therefore an increased friction factor f in the channel compared to a smooth duct. Fig. 9 shows the experimental results for the friction factor for the different rib configurations under investigation. Friction factors can reach values, which are more than 25 times higher than the value for a smooth channel. This shows that the ribs strongly influence the flow field in the channel, leading to intensified mixing and high turbulence in the flow. From Fig. 9 one sees that the ribs for case 1 with 45 deg. inclined ribs (without ribs in the arc area) have the lowest friction factor. However, this friction factor is about 15 times lager than the one for the smooth duct. Changing the rib angle for case 1 to 60 deg. leads to a further substantial increase in friction factor by about 50%. This is caused by the changed secondary flow structure for the 60 deg. ribs. If ribs are introduced into the arc area, the friction factor increases compared to case 1. The largest increase can be observed by introducing double-sided diagonal arc ribs (case 5), which run around the leading edge or double-sided orthogonal ribs (case 3). However this increase in friction factor is moderate (about 15%) as compared to case 1. This means that a change of the rib type in the arc area leads only to relatively moderate changes in the overall friction factor, compared to a change in rib angle from 45 to 60 deg. This result is obvious, because of the small percentage of the ribbed perimeter occupied by the arc area. For case 3 also higher ribs ($e/H = 0.15$) have been tested. It can be seen from Fig. 9 that the friction factor for case 3b increases by about 40% as compared to case 3a. Changing finally the rib pitch from $P/e_{\min} = 15$ to 20 (case 3 and case 3a) has only a small effect on the friction factor, which is visible in Fig. 9.

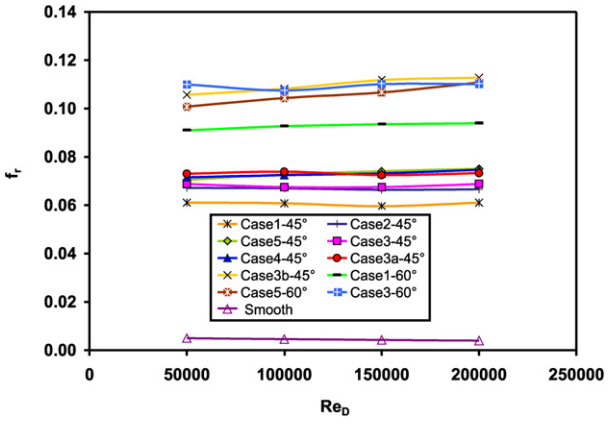

Fig. 9. Friction factor for different rib configurations as a function of the Reynolds number.

3.2.2. Heat transfer results

From the liquid crystal measurements, the full two-dimensional distribution of the heat transfer coefficients is obtained after evaluation. This information is very useful, in order to understand the different rib configurations. Such plots are shown in Fig. 10. All plots have the same color range and thereby the same scale for the heat transfer coefficients in order to facilitate comparison. It can be seen that strong differences in the local structures of the heat transfer coefficients exist. This is caused by the different secondary flow structures, which are driven from the ribs near the leading edge arc. It is visible that case 5 – 60° leads to high heat transfer coefficients in the arc area, where the highest heat load from the outside will occur. On the other hand, it can be seen that using only a single sided orthogonal rib in the arc (case 4 – 45°) results in relatively low values of the heat transfer coefficient in this area. This is obvious, because the distance between the arc rib is now too large in order to guarantee a good heat transfer enhancement. Furthermore this figure illustrates nicely how the local rib structures in the arc area can be used in order to influence the position of the maximum heat transfer coefficient. Comparing for example case 5 – 45° with case 4 – 45°, it is obvious that case 5 provides a more uniform distribution of the local heat transfer coefficients in the arc area. In Fig. 11, the local values of the Nusselt number are averaged from rib to rib (for a fixed position of the local coordinates) and are plotted as a function of the local coordinate around the circumference of the channel. These area averaged values of the Nusselt number are useful in understanding the local heat transfer behavior. Fig. 11 shows clearly that the rib configuration case 1 results in relatively low heat transfer coefficients in the leading edge arc. This is obvious, because this configuration has no arc ribs (see Fig. 6). Introducing double sided orthogonal half arc ribs results in a moderate heat transfer enhancement in the leading edge arc (case 2). By changing the rib structure in the arc region, the local heat transfer can be enhanced even more. Case 5 shows that high values of the Nusselt number can be achieved by using double-sided diagonal arc ribs. However, this results in slightly decreasing Nusselt numbers on the suction side. A good compromise is case 3, which results in high Nusselt numbers in the arc area as well as on the pressure and suction side. The results presented here show clearly that the rib structure in the arc area can be adapted to guarantee sufficient cooling.

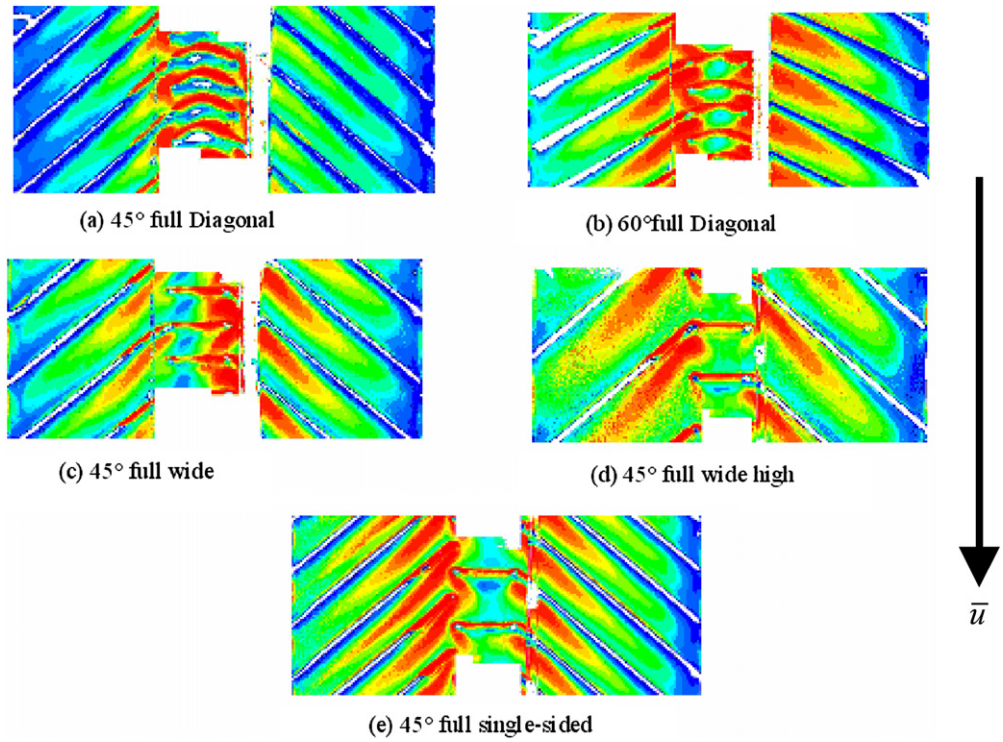

Fig. 10. Two-dimensional Nusselt number distributions for $Re_D = 100\,000$.

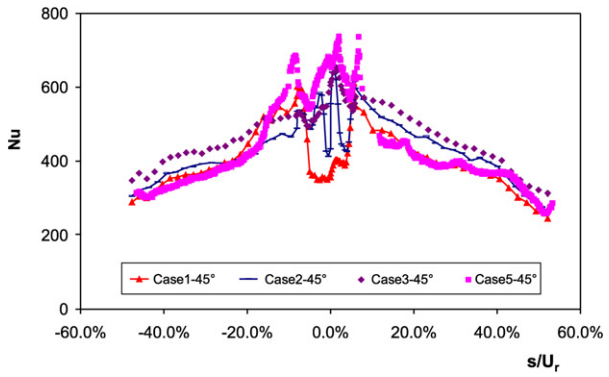

Fig. 11. Local distribution of the Nusselt number around the circumference of the duct for $Re_D = 100\,000$.

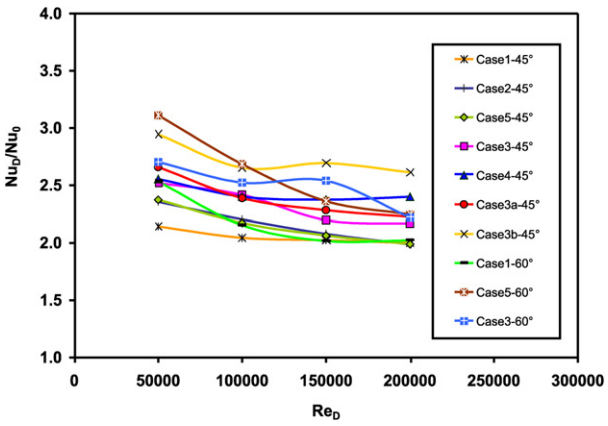

Fig. 12. Averaged Nusselt number ratio as a function of the Reynolds number.

Fig. 12 shows the heat transfer enhancement for all different rib configurations as a function of the Reynolds number. For obtaining this plot, the Nusselt number has been averaged over the whole area between two individual ribs. The averaged Nusselt numbers are based on the Nusselt number for the smooth channel, Eq. (6), which is proportional to $Re_D^{0.8}$. It can be seen that the heat transfer enhancement decreases with increasing values of the Reynolds number. This is a well-known behavior for ribbed channels (see for example [4]). As it can be seen from Fig. 12, the highest heat transfer enhancement can be obtained for case 5 – 60° ribs. The other 60 deg. ribs (case 1, case 3) result in smaller heat transfer enhancements. Comparable to case 5 – 60° is the heat transfer enhancement for 45 deg. ribs by using increased rib heights ($e/H = 0.15$, case 3b). For this case the decrease in heat transfer enhancement with increasing Reynolds number is not as strong as for the 60 deg. ribs (case 5 – 60°). By taking into account that the friction factors for the 60 deg. ribs are very similar to case 3b, the high 45 deg. ribs are a good solution if high heat transfer enhancement is needed for larger values of the Reynolds numbers and if no restriction on the overall pressure drop is given.

3.3. Rib performance

In order to compare the different rib configurations, the heat transfer enhancement, as well as the increase in pressure drop, needs to be considered. This can be done, by plotting the heat transfer enhancement Nu_D/Nu_0 as a function of the friction factor ratio f/f_0. This is shown in Fig. 13. Each data point in this chart denotes one specific Reynolds number. From Fig. 13 it can clearly be seen that highest heat transfer enhancement ratios can

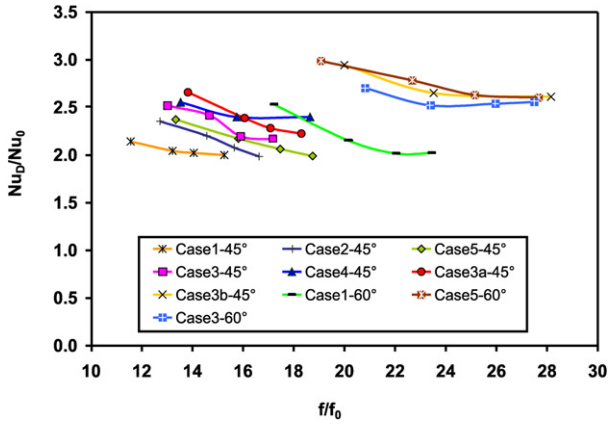

Fig. 13. Nusselt number ratio as a function of the friction factor ratio.

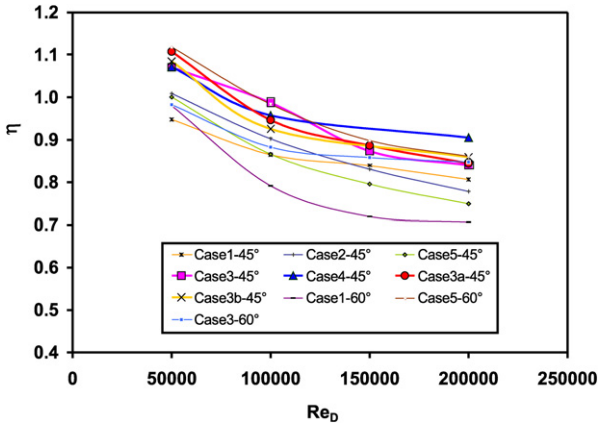

Fig. 14. Mean values of the thermal performance as a function of the Reynolds number.

be achieved with 60 deg. ribs (case 5), which also result in the highest overall values of f/f_0. From Fig. 13 one sees clearly that using 60 deg. ribs or high 45 deg. ribs (case 3b – 45°) results in overall heat transfer enhancement ratios up to about three. This is very large, if one considers the high Reynolds numbers investigated in this study. However, for these cases, the friction factor increases to values of about 20–28 times larger than the one for a smooth channel. Therefore, these rib types are only interesting for blade designs, where the pressure drop is no limiting factor of the design. For normal blade designs, cases 3 and 4 seem to be the superior rib configurations, because the overall heat transfer enhancements of about 2.5 can be achieved with acceptable increase in friction factors. Coming back to Fig. 10, it can be seen that case 4 provides relatively low heat transfer coefficients in the arc area. Therefore, this rib type is also not optimum for leading edge blade cooling. Thus case 3 was found to the optimum rib structure from all investigated rib configurations of the present study.

In order to evaluate the rib performance for the usage in heat exchangers, it is common to compare the heat transfer enhancement at a constant pumping power [4]. This results in the so-called thermal efficiency

$$\eta = \frac{St/St_0}{(f/f_0)^{1/3}} \tag{8}$$

Because the ribbed and smooth channel are subjected to the same Reynolds and Prandtl number, Eq. (8) reduces to

$$\eta = \frac{Nu_D/Nu_0}{(f/f_0)^{1/3}} \tag{9}$$

Fig. 14 shows the thermal efficiency as a function of the Reynolds number for all investigated rib designs. Here it can be seen that η decreases with increasing values of the Reynolds number. Furthermore, one can see clearly in this figure how the different rib configurations perform. For example, it can be seen that in general the 60 deg. ribs result in lower thermal efficiency as the 45 deg. ribs, because the associated pressure loss is higher for these kind of rib configurations. Once again, it can be seen that rib configuration case 3 reaches highest values of η. This supports the conclusions drawn from the previous figures and shows clearly that this rib configuration is the optimum from the present investigated rib designs.

4. Conclusions

The present investigation has been concerned with new rib designs, which have a locally changing rib height in the channel. These ribs are very useful for duct geometries with restricted flow areas. Based on the experimental results presented in this paper, the following main conclusions might be drawn:

- The new rib configurations, with locally changing rib heights, provide high heat transfer augmentations, even in the arc of the leading edge. The overall heat transfer enhancements depend on the rib angle and also on the rib structure in the arc area. It was found that 60 deg. ribs provide the highest overall heat transfer coefficients, but lead also to extremely high friction factors.
- Examining the local distribution of the heat transfer coefficients in the arc area shows that double-sided orthogonal arc ribs (case 3) and double-sided diagonal arc ribs (case 5) are superior, because they provide homogeneous and high heat transfer coefficients in the arc area.
- Considering the local distribution of the heat transfer coefficients as well as the overall heat transfer enhancement and the increase in friction factor, rib case 3 (double-sided orthogonal arc ribs) with 45 deg. inclination are found to be the optimum rib arrangement for the leading edge channel of an industrial gas turbine blade.

Acknowledgements

The financial support of the present investigation by ALSTOM is greatly acknowledged. Additionally, the authors would like to thank Dr. S. Parneix (ALSTOM) for many helpful discussions concerning the present investigation.

References

[1] J.C. Han, S. Dutta, Internal convection heat transfer and cooling: An experimental approach, VKI-LS 1995-05, Heat Transfer and Cooling in Gas Turbines, 1995.
[2] M.E. Taslim, Convective cooling in non-rotating and rotating channels – Experimental aspects, VKI-LS 2000-03, Aero-Thermal Performance of Internal Cooling Systems in Turbomachines, 2000.

[3] P.M. Ligrani, M.M. Oliveira, T. Blaskovich, Comparison of heat transfer augmentation techniques, AIAA Journal 41 (2003) 337–362.

[4] J.C. Han, S. Dutta, S.V. Ekkad, Gas Turbine Heat Transfer and Cooling Technology, Taylor & Francis, London, 2001.

[5] J.C. Han, Y.M. Zhang, C.P. Lee, Augmented heat transfer in square channels with parallel, crossed and V-shaped angled ribs, ASME J. Heat Transfer 113 (1991) 590–596.

[6] J.C. Han, Y.M. Zhang, High performance heat transfer ducts with parallel broken and V-shaped broken ribs, Int. J. Heat Mass Transfer 35 (1992) 513–523.

[7] D.E. Metzger, R.P. Vedula, D.D. Brenn, The effect of rib angle and length on convection heat transfer in rib-roughened triangular ducts, in: ASME/JSME Thermal Engineering Joint Conference, 1987.

[8] D.E. Metzger, R.P. Vedula, Heat transfer in triangular channels with angled roughness ribs on two walls, Experimental Heat Transfer 1 (1987) 31–44.

[9] Y.M. Zhang, W.Z. Gu, J.C. Han, Augmented heat transfer in triangular ducts with full and partial ribbed walls, J. Thermophys. Heat Transfer 8 (1994) 574–579.

[10] A. Haasenritter, B. Weigand, Heat transfer in triangular rib-roughened channels, in: Proc. of the 35th National Heat Transfer Conference, Anaheim, CA, USA, NHTC01-1512, 2001.

[11] M.E. Taslim, T. Li, S.D. Spring, Measurements of heat transfer coefficients and friction factors in rib-roughened channels simulating leading-edge cavities of a modern turbine blade, ASME J. Turbomachinery 119 (1997) 601–609.

[12] B. Weigand, K. Semmler, J. von Wolfersdorf, Heat transfer technology for internal passages of air-cooled blades for heavy-duty gas turbines, Ann. New York Acad. Sci. 934 (2001) 179–193.

[13] K. Hall, B. Johnson, B. Weigand, P.S. Wu, Coolable blade, United States Patent, Patent Number: 5919031, 1999.

[14] A. Beeck, B. Johnson, B. Weigand, P.S. Wu, Cooling system for the leading edge of a hollow blade for a gas turbine, European Patent, EP0892149, 1997.

[15] M. Amro, A. Haasenritter, B. Weigand, An experimental and numerical study of heat transfer and pressure drop in a rib-roughened triangular duct, in: Conference on Turbomachinery Fluid Dynamics, Prague, 2003.

[16] Z. Wang, D.R.H. Gillespie, P.T. Ireland, Advances in heat transfer measurements using liquid crystals, in: Engineering Foundation, Heat Transfer, San Diego, 1996.

[17] G. Vogel, Experimental study on a heavy film cooled nozzle guide vane with contoured platforms, PhD thesis, No. 2602, Swiss Federal Institute of Technology, Lausanne, Switzerland, 2002.

[18] J.W. Baughn, X. Yan, Liquid crystal methods in experimental heat transfer, in: Proceedings of 32nd Heat Transfer and Fluid, Mechanics Institute Sacramento, California, 1991, pp. 14–40.

[19] T.V. Jones, Z. Wang, P.T. Ireland, The use of liquid crystals in aerodynamic and heat transfer experiments, in: Proceedings of the First I. Mech. E. Seminar on optical methods and Data Processing in Heat and Fluid Flow, City University, London, 1992, pp. 51–65.

[20] S.V. Ekkad, J.C. Han, A transient liquid crystal thermography technique for gas turbine heat transfer measurements, Measurement Sci. Technol. 11 (2000) 957–968.

[21] G. Wagner, M. Kotulla, P. Ott, B. Weigand, J. von Wolfersdorf, The transient liquid crystal technique: influence of surface curvature and finite wall thickness, ASME J. Turbomachinery 127 (2005) 175–182.

[22] J. Nikuradse, Untersuchungen über turbulente Strömungen in nicht kreisförmigen Rohren, Ingenieur-Archiv (1930) 306–332.

[23] W.M. Kays, M.E. Crawford, B. Weigand, Convective Heat and Mass Transfer, McGraw-Hill, New York, 2004.

[24] J. von Wolfersdorf, R. Hoecker, C. Hirsch, A data reduction procedure for transient heat transfer measurements in long internal cooling channels, ASME J. Heat Transfer 120 (1998) 314–321.